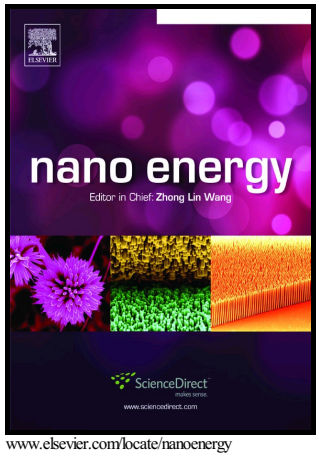

www.elsevier.com/locate/nanoenergy

MoSSe@reduced Graphene Oxide Nanocomposite Heterostructures as Efficient and Stable Electrocatalysts for the Hydrogen Evolution Reaction

Bharathi Konkena, Justus Masa, Wei Xia, Martin Muhler, Wolfgang. Schuhmann

PII: S2211-2855(16)30072-6
DOI: http://dx.doi.org/10.1016/j.nanoen.2016.04.018
Reference: NANOEN1223

To appear in: *Nano Energy*

Received date: 19 January 2016
Revised date: 10 April 2016
Accepted date: 13 April 2016

Cite this article as: Bharathi Konkena, Justus Masa, Wei Xia, Martin Muhler and Wolfgang. Schuhmann, MoSSe@reduced Graphene Oxide Nanocomposite Heterostructures as Efficient and Stable Electrocatalysts for the Hydrogen Evolution Reaction, *Nano Energy* http://dx.doi.org/10.1016/j.nanoen.2016.04.018

MoSSe@reduced Graphene Oxide Nanocomposite Heterostructures as Efficient and Stable Electrocatalysts for the Hydrogen Evolution Reaction

Bharathi Konkena[a] , Justus Masa[a] , Wei Xia[b], Martin Muhler[b] , Wolfgang Schuhmann[a] *

[a] Analytical Chemistry - Center for Electrochemical Sciences (CES) Ruhr-Universität Bochum; Universitätsstr. 150, D-44780 Bochum (Germany)
E-mail: wolfgang.schuhmann@rub.de

[b] Laboratory of Industrial Chemistry; Ruhr-Universität Bochum; Universitätsstr. 150, D-44780
Bochum (Germany)

Abstract

Non-noble metal based materials efficiently catalyzing the hydrogen evolution reaction (HER) are reported based on a novel strategy where electrocatalytically active ultrathin molybdenum sulphoselenide sheets are incorporated into electrically conducting reduced graphene oxide sheets via a self-assembly approach. By taking advantage of the electrostatic attraction between the two oppositely charged nanosheets, MoSSe@*r*GO composite materials are obtained exhibiting superior electrocatalytic activity and stability for the HER allowing a current density of 5 mA cm^{-2} at a low overpotential of only 135 mV. These findings pave the way to novel electrocatalysts based on composites of MoSSe and reduced graphene oxide towards the design of ultra-light, mechanically robust and electrically conductive electrode materials for electrocatalytic water splitting.

Key words: MoSSe nanosheets, reduced graphene oxide, self-assembly, MoSSe@*r*GO composites, hydrogen evolution reaction

1. Introduction

In recent years, one of the most pursued scientific challenges is providing adequate energy to meet present and future energy needs through environmentally clean processes. Noble metal based catalysts such as Pt and Pd and their alloys are the most active hydrogen evolution catalysts achieving very low overpotentials for water splitting [1-5]. Considering the limited availability and high cost of precious metal catalysts, it is highly desirable to find alternative high efficiency and stable non-precious metal catalysts. Towards this aim, layered transition

metal oxides [6,7], nitrides [8], phosphides [9-13] and chalcogenides [14,15] have attracted widespread attention as catalyst materials for energy applications. In particular, layered transition metal chalcogenides (TMCs) such as MoS_2 [16,17], $MoSe_2$ [18], WS_2 [19], WSe_2 [20], NiS_2 and CoS_2 [15,21] have been explored as potential electrode materials for electrochemical H_2 evolution. The electrocatalytic properties of such non-precious metal electrocatalysts can be tuned by varying the sulphur/selenium ratio making them attractive for various energy conversion applications [22–25].

Two dimensional (2D) nanosheets which are typically flat or slightly corrugated flexible sheets provide a relatively higher amount of exposed active edge sites [26,27]. However, poor intrinsic conductivity and electron transport greatly limit their use in electrocatalytic applications. On the other hand, these 2D nanosheets can easily restack and by this eventually lose their catalytic activity. Furthermore, the catalytic performance of these materials is improved by tethering them to highly conducting materials (like graphene or carbon nanotubes) [28,29] thereby exposing more active sites for facilitating fast electron transport. Several strategies have been suggested previously to achieve this goal, most of them involving TMC nanosheets directly grown on reduced graphene oxide (*r*-GO) sheets by solvothermal synthesis. For instance, MoS_2/*r*GO and $MoSe_2$/*r*GO composites exhibit a high abundance of catalytic edge sites and outstanding HER activity [30,31]. Three dimensional CoS_2 and $CoSe_2$/graphene hybrid heterostructures are excellent HER catalysts [32,33]. Furthermore, recent studies reported a methodology based on "chemical tuning" to improve the activity of MoS_2 [34,35]. Alloyed nanoflakes especially with the chemical composition of MoSSe exhibit improved performance in terms of both activity and stability in comparison to either MoS_2 or $MoSe_2$ [22–25]. It was suggested that the introduction of Se modulates the d-band electronic structure of Mo, leading to tuning of the hydrogen adsorption free energy and consequently the electrocatalytic activity.

Here, we propose the combination of two colloidal nanosheet systems with opposite charges to achieve spontaneous self-assembly through electrostatic interactions [36]. One of the starting materials, i.e. exfoliated MoSSe nanosheets, in the presence of a cationic surfactant is known to be an active HER catalyst. The second material is graphene oxide (GO), consisting of a unique combination of hydrophilic groups and hydrophobic graphitic domains coexisting on a single GO sheet [37,38]; which provides the basis for its selection as graphene precursor [39]. GO sheets are typically negatively charged in water as a consequence of the deprotonation of the functional groups at the surface [40]. Owing to electrostatic attractions, GO sheets are supposed to self-assemble with positively charged exfoliated MoSSe sheets in

aqueous solution to yield electrically neutral hybrids. We demonstrate the self-assembly of exfoliated cationic MoSSe sheets and anionic GO sheets followed by solvothermal treatment to form a layered hybrid exhibiting remarkable HER activity and stability. The developed catalyst requires an overpotential of as low as 135 mV for generating a current density of 5 mA cm^{-2} during HER and it exhibits a Tafel slope of only 51 mV/dec.

2.0 Materials and methods

2.1 Synthesis of MoSSe crystals

Bulk MoSSe crystals were synthesized by the chemical vapor transport method [41]. In a typical synthesis, elemental powders of Mo, S and Se were mixed in the required stoichiometric proportions and inserted into a quartz tube. The quartz tube was evacuated to ~10^{-6} mbar and sealed. The sealed quartz tube was placed in a tube furnace at 800 ºC for 2 weeks to ensure crystal formation. The quartz tube was cooled down to room temperature and opened for collecting the obtained crystals. For comparison, MoS_2 and $MoSe_2$ bulk crystals were synthesized under similar conditions.

2.2 Liquid exfoliation of bulk MoSSe into nanosheets

Bulk layered MoSSe crystals were exfoliated by dispersing 5 mg mL^{-1} of the crystals in a CTAB surfactant solution (2mg mL^{-1}) in water followed by sonication for 10 h in a 100 W bath sonicator. After sonication, the dispersions are subjected to differential centrifugation to narrow down the size distribution. For this, the dispersions were centrifuged at 1000 rpm for 1 h, and the supernatant was separated and subjected to successive centrifugation at 2000 and 4000 rpm for periods of 2 h. The process is terminated at this stage (at 4000 rpm); the sediment is collected and redispersed in water under sonication. After sonication the dispersion was stable for 3 months without any flocculation and used for further investigations. A similar strategy applied for exfoliating the MoS_2 and $MoSe_2$ bulk crystals.

2.3 Synthesis of GO and reduced-GO (*r*-GO)

Oxidation of graphite: GO was prepared from graphite using a modified Hummers method [42,43]. In a typical reaction, 0.25 g of graphite powder and 46 mL of concentrated H_2SO_4 were stirred in an ice bath by maintaining the temperature below 5^oC followed by slow addition of 6 g of $KMnO_4$. After the complete addition of $KMnO_4$, the solution was transferred to a water bath at 37^oC and the water was allowed to evaporate until it formed a thick paste. This paste was subsequently diluted with excess of water (approximately 95 mL) and then stirred at 95^oC for 15-20 min. Finally, 280 mL of water was added followed by the

slow addition of 20 mL of 30% H_2O_2 with constant stirring. At this time, the solution turns from dark brown to yellow. The mixture was allowed to settle overnight and the supernatant was decanted. The precipitate was washed with 10% HCl (100 mL) until the precipitate was free from sulphate ions and the brownish solution was allowed to settle overnight. The process was repeated until the dispersion was neutral. The dispersion was centrifuged and the precipitate was dried in a desiccator under vacuum.

Reduction of GO: 75 mg of GO were dispersed in 50 mL water under sonication for 2 h. 1 mL ammonia was added to reach pH 10 and the mixture was transferred to a 60 mL autoclave where it was heated at 150^{o}C for 24 h. The reduced GO gradually precipitated as a black solid. The precipitate was removed, washed with milliQ water and then dried under vacuum.

2.4 Synthesis of MoSSe@ *r*GO composites

250 mg of the exfoliated MoSSe sheets were dispersed in a beaker containing 75 mg of an aqueous dispersion of GO, and the resulting mixture was stirred for 4 h to ensure spontaneous assembly of the negatively charged GO sheets with the positively charged MoSSe nanosheets. Further reduction was carried out by transferring the mixture into a 60 mL Teflon-lined autoclave. The autoclave was sealed and heated at 150°C for 24 h in an oven and then cooled down to room temperature. The precipitate was collected by centrifugation and washed several times with ethanol-water mixture (1:2) before it was dried in vacuum at 60°C overnight.

2.5 Electrochemical measurements

All electrochemical measurements were performed using an Autolab potentiostat/galvanostat (PGSTAT12) in a conventional three-electrode cell in combination with a Metrohm RDE-2 rotator. A glassy carbon disc of a geometric area of 0.126 cm^2 modified with the catalysts was used as the working electrode, a Ag/AgCl/3M KCl as reference electrode and a Pt mesh as counter electrode. The reference electrode was calibrated with respect to the reversible hydrogen electrode (RHE). Prior to experiments, the glassy carbon electrode was polished on a polishing cloth using different alumina pastes (3.0 - 0.05 μm) to obtain a mirror-like surface, followed by ultrasonic cleaning in water. For electrochemical measurements a catalyst ink was prepared by dispersing 5.0 mg mL^{-1} of the catalyst in water under ultrasonication for 30 min. 5.0 μL of the catalyst suspension was drop-coated onto the polished glassy carbon electrode and dried in air at room temperature. Before the HER measurements, the modified electrodes were subjected to continuous potential cycling in the potential window of -0.5V –

0.5 V until reproducible voltammograms were obtained. Electrochemical impedance spectroscopy was recorded at the corresponding open circuit potential using an ac perturbation of 10 mV_{pp} in the frequency range from 50 kHz to 1 Hz. The solution resistance was determined from the resulting Nyquist plot, and later used for the ohmic drop correction according to the relation, $E_c = E_m - iR_s$, where E_c is the corrected potential and E_m is the measured potential. All current densities were calculated using the geometric surface area of the electrode. All potentials were rescaled to the pH-independent reversible hydrogen electrode (RHE). The long-term stability was evaluated chronopotentiometrically at a current density of -10 mA cm^{-2} on a graphite rotating disk electrode (5 mm diameter) modified with the catalyst in 0.5 M H_2SO_4 solution. During the measurements, the electrode was maintained at a rotation of 400 rpm to avoid accumulation of gas bubbles on the electrode surface. The catalyst loading for each electrode was 0.198 mg cm^{-2}. The electrolyte was purged for ~20 min with Ar prior to measurements and an Ar gas stream was maintained over the electrolyte throughout the timeframe of the experiment. All the measurements were carried out at room temperature.

3. Results and Discussion

Bulk MoSSe crystals were synthesized by means of the chemical vapor transport method and further subjected to long-term ultra-sonication in water for 6 h to exfoliate the MoSSe crystals into nanosheets in the presence of the cationic surfactant cetyltrimethylammonium bromide (CTAB). The resulting aqueous dispersions were subjected to differential centrifugation to narrow down the size distribution to separate the exfoliated nanosheets into different sized MoSSe sheets in a density gradient (Figure S1). The exfoliated MoSSe sheets (5 mg mL^{-1}) were re-dispersed in an aqueous GO dispersion (1.5 mg mL^{-1}). The resulting mixture was heated to 150^{o}C for 24 h to ensure assembly of GO with exfoliated MoSSe sheets followed by reduction of GO. Figure 1a shows the magnitude of the surface charge of the nanosheets derived from the zeta potential distribution. Exfoliated MoSSe nanosheets exhibit an overall positive charge (ζ ~ 40 mV) to stabilize the colloid, whereas GO sheets exhibit a negative charge (ζ ~ -36 mV). The dispersions are stable for about 6 months (Figure S2). These oppositely charged nanosheets undergo spontaneous assembly due to electrostatic attraction [36]. Simultaneously, the electronic conductivity is partially restored upon reduction of GO removing partially the oxygen functionalities. The resulting MoSSe@*r*GO composites were characterized by XRD, Raman and XPS measurements. X-ray diffraction patterns of the MoSSe nanosheets display the expected characteristic hexagonal 2H-molybdenum dichalcogenide features and the reflections perfectly match the reported reference patterns of

$MoS_{1.0}Se_{1.0}$ (JCPDF no. 36-1408). The highly intense (103) reflections indicate gradual expansion of the unit cell along the c-axis upon substitution of the Se atoms (Figure S3). Moreover, for the exfoliated MoSSe and MoSSe@ *r*GO composites, all diffraction peaks are broadened indicating a decrease in structural crystallinity, increase of disorder or defect density as well as decrease in the particle size (Figure 1b).

Raman spectra of MoSSe nanosheets (Figure 1c) revealed the characteristic Mo-S and Mo-Se bands that are different from the MoS_2 and $MoSe_2$ bands because of Se substitution, effectively weakening the Mo-S bond strength in MoSSe (Figure S4). In Figure 1c, the MoSSe@ *r*GO composite also displays similar features along with the carbon G and D bands with enhanced I_D/I_G ratio as compared to graphene oxide (Figure S5), indicative of restoration of sp^2 domains upon reduction. Further chemical insight into the structure of MoSSe@ *r*GO composites and MoSSe exfoliated nanosheets was obtained by X-ray photoelectron spectroscopy (XPS). Representative XPS results of the Mo 3d core levels of MoSSe and MoSSe@ *r*GO are shown in Figure 1d. The Mo 3d core level spectra of MoSSe nanosheets consist of $3d_{5/2}$ and $3d_{3/2}$ peaks centered at 229.2 eV and 232.4 eV, respectively, characteristic of Mo^{4+} in the hexagonal 2H phase [22]. These binding energies are significantly lower compared to the corresponding Mo-3d bands of MoS_2 (Figure S7) suggesting that the d-band electronic structure of MoSSe is substantially modified by substitution of the more electronegative S atoms with the less electronegative Se [22-25]. Notably, relative changes were also observed in the S 2p and Se 3d XPS spectra upon increasing the Se content (Figure S6). Moreover, an appreciable negative shift in the binding energies of the Mo 3d spectra was observed for the MoSSe@ *r*GO composites (Figure 1d). The changes in the Mo 3d binding energies in the composite prompt us to speculate that there is a substantial interaction between the *r*-GO π-electrons and the MoSSe *d*-orbitals, which effectively change the *d*-band electronic structure and consequently the electrocatalytic HER activity (Figure S8). The MoSSe@ *r*GO composite also displayed a highly intense C 1s peak, which is characteristic for C=C bonding in graphitic carbon while the intensities corresponding to the oxygen functional groups, C-O and C=O, were substantially reduced, indicative of partial restoration of sp^2 domains (Figure S9).

The surface morphology was examined by AFM, SEM and TEM analysis. SEM images of bulk MoSSe (Figure S10) showed crystals of several micrometers in size (50 μm), while for exfoliated MoSSe sheets (Figure 2a) a 2D-nanosheets-like morphology was revealed. For the MoSSe@ *r*GO composite (Figure 2c), the 2D-MoSSe nanosheets are uniformly distributed on the *r*GO sheets. Energy dispersive X-ray spectroscopy data provides corroborative evidence

of a $MoS_{1.0}Se_{1.0}$ stoichiometry in the composite, indicating that the stoichiometry does not change in the MoSSe@ *r*GO composite (Figure S11 and Figure S12).

The AFM and TEM images of the MoSSe sheets confirmed the successful exfoliation of bulk MoSSe into nanosheets (Figure 2b). The thickness of the MoSSe nanosheets was found to be about 2 nm indicative of two layers (Figure S13). The TEM image of MoSSe@ *r*GO (Figure 2d) shows the MoSSe nanosheets distributed on *r*-GO in the hybrid nanostructure. The crystal structure of MoSSe@ *r*GO was examined by high resolution TEM (HRTEM). A magnified TEM image of a MoSSe monolayer is shown in Figure 3a, and the corresponding HRTEM image displayed clear crystal lattice fringes with an interplanar spacing of ~0.28 nm (Figure 3c) [23]. Similar structural features were also observed for the surface structure of MoSSe@ *r*GO (Figure 3f), including an amorphous phase of *r*-GO in the background. Figure 3 provides additional evidence of the ultrathin 2D-MoSSe nanosheets uniformly distributed on the *r*-GO sheets.

The electrocatalytic performance in the HER of as exfoliated MoSSe sheets and MoSSe@ *r*GO were investigated by rotating disk electrode (RDE) measurements in Ar-saturated 0.5 M H_2SO_4 at a scan rate of 5 mVs^{-1}. Nanosheets were drop-coated on a glassy carbon electrode without any binder and used as working electrode. For comparison, MoS_2, $MoSe_2$ and *r*-GO samples were also evaluated under identical conditions. The iR-corrected linear sweep voltammograms of the HER of the investigated catalysts are shown in Figure 4. MoSSe nanosheets exhibit improved electrocatalytic HER activity with a low overpotential of 240 mV achieving a current density of 5 mA cm^{-2} in comparison to either MoS_2 or $MoSe_2$ nanosheets (Figure 4a). It has been suggested that an improved HER activity likely results from the higher intrinsic activity of the alloyed catalysts due the hydrogen adsorption free energy being closer to the thermodynamically neutral value [22,23]. It is worth noting that the results are comparable to those reported for MoS_2 or $MoSe_2$ nanosheets previously [22-24]. Compared to exfoliated MoSSe sheets, the overpotential of the MoSSe@ *r*GO composite nanostructures further shifted to 135 mV at a current density of 5 mA cm^{-2}, suggesting that the enhanced catalytic activity is realized due to the superior electron transfer efficiency in MoSSe@ *r*GO composites caused by the intrinsic electronic conductivity of *r*-GO. Similar experiments were performed using a physical mixture of MoSSe with *r*-GO sheets, which exhibited a much lower HER activity (Figure S16). The enormous difference in HER activity between the physical mixture of MoSSe with *r*-GO and the MoSSe@ *r*GO nanocomposite is attributed to the intimate chemical and electronic coupling between the catalytically active MoSSe nanosheets and the highly conducting *r*-GO sheets. In addition, MoSSe@ *r*GO

nanostructures revealed a low overpotential of 153 mV at a current density of 10 mA cm^{-2} , being much smaller than for MoS_2/*r*GO [30] and $MoSe_2$/ *r*GO (195 mV) [31] hybrid nanostructures at the same current density, thus highlighting the excellent catalytic performance by the MoSSe@ *r*GO composite. A comparison of the HER activity of MoSSe@ *r*GO with molybdenum based HER catalysts reported in the literature is given in Table S1. These results underpin the importance of assembling catalytically active MoSSe nanosheets with conducting carbon at the molecular level for designing high performance electrode materials for electrocatalytic applications.

Volmer: $H_3O^+ + e^- \longrightarrow H_{ads}$	(120 mV)	(1)
Heyrovsky: $H_{ads} + H^+ + e^- \longrightarrow H_2$	(40 mV)	(2)
Tafel: $H_{ads} + H_{ads} \longrightarrow H_2$	(30 mV)	(3)

The Tafel slope was determined to interpret the elementary steps involved in the HER kinetics. Tafel plots were fitted to the equation $\eta = b \log j + \log j_0$ (overpotential η, current density j, Tafel slope b, and exchange current density j_0). The HER mechanism in acidic electrolytes typically involves three major steps [5, 44].

The Tafel slope of the HER on Pt is about 29 mV per decade, close to the theoretical value (b = 2.3RT/2F), corresponding to Volmer–Tafel steps, with the recombination step (3) being the rate-limiting step at low overpotentials. Tafel slopes of ~51 and 63 mV per decade were obtained for the MoSSe@ *r*GO composite and MoSSe sheets, respectively. Tafel slopes between 50 to 60 mV per decade are attributed to a fast discharge reaction (1) followed by a rate limiting recombination step (3), where the chemisorption of hydrogen from aqueous solution onto the surface requires little activation energy [45]. In the rate-limiting step, the adsorbed hydrogen atoms migrate over the electrode surface to interact with immobile adsorbed atoms to form molecular hydrogen (spillover effect) [23,45]. The relatively lower Tafel slope observed for the MoSSe@ *r*GO composite nanostructures is indicative of faster reaction kinetics during hydrogen evolution as compared to MoSSe nanosheets. The size of the MoSSe nanosheets was not altered after formation of the composite with *r*-GO. The conducting *r*-GO sheets may facilitate the adsorption of hydrogen near the catalytically active edge sites thus playing a role in improving the kinetics leading to a possible change in the mechanism from pure MoSSe to the MoSSe@ *r*GO composite. MoSSe sheets are uniformly distributed at the *r*-GO sheets and effectively lower the aggregation tendency, thus making it possible to maximize the exposed active edges. In addition, *r*-GO sheets act as an electrically

conducting 2D-matrix to improve the charge transfer efficiency. It has been demonstrated that electrocatalytic activity and electronic conductivity are improved when *r*-GO is used as a catalyst support in fuel cells and water electrolyzers [32,46]. Although extensively studied, the physical origin of the electrocatalytic activity enhancement with *r*-GO remains unclear. However, theoretical studies concluded that the electronic band structures of graphene are significantly affected by a large wave function overlap between metal d-states and graphene π-electrons, resulting in a small band gap (2 meV) with randomly distributed metallic states [47,48]. This highlights a new route to design devices with both finite band-gap and high carrier mobility.

Stability is one of the key factors in evaluating catalyst performance. To assess the stability of MoSSe and MoSSe@*r*GO during HER, continuous cyclic voltammograms to up to 5000 cycles, and galvanostatic polarization curves at a current density of -10 mA cm^{-2} were recorded. Figure 4d displays iR-corrected LSV curves recorded at 5 mV s^{-1} for MoSSe@*r*GO before and after performing 5000 continuous cyclic voltammograms between 0.0 V and -0.5 V. Notably, no appreciable activity change was observed after 5000 cycles indicating excellent stability of the MoSSe@ *r*GO composite nanostructure during HER. This observation further suggests that the MoSSe@ *r*GO structure remains intact with the MoSSe nanosheets firmly anchored on the surface of *r*-GO. The potential required to deliver a current density of 10 mA cm^{-2} is an important figure of merit for the viability of a HER catalyst, because it corresponds to the current density required to attain 10 % efficiency in a solar-to-fuel conversion device [49]. Galvanostatic measurements also demonstrated outstanding stability of the MoSSe@ *r*GO nanostructures in acidic media (inset of Figure 4d), confirming the synergetic effect arising from the electrostatic interactions between the MoSSe and *r*-GO nanosheets effectively improving the charge transfer efficiency through the unique structure. Corroborative evidence of its high electrical conductivity was obtained from electrochemical impedance spectroscopy measurements. The charge transfer resistance (R_{ct}) of the MoSSe@ *r*GO composite determined from Nyquist plots was ~43.2 Ω which is significantly lower than that for MoSSe ~102.4 Ω (Figure S17).

4. Conclusions

A MoSSe@ *r*GO composite synthesized by self-assembly of cationic MoSSe and anionic *r*-GO nanosheets provides a uniform distribution of catalytically active MoSSe nanosheets on electrically conducting *r*-GO sheets which synergistically maximize the exposed active edges and enhance electron transfer. The MoSSe@ *r*GO composite exhibited outstanding HER

activity and stability requiring as low as 135 mV overpotential to deliver a current density of 5 mA cm^{-2}. The Tafel slope of the HER at MoSSe@ *r*GO was 51 mV per decade indicating that the kinetics of the reaction was limited by recombination of adsorbed hydrogen rather than by charge transfer. Our findings pave a facile route to design novel electrocatalysts based on composites of molybdenum sulphoselenides and reduced graphene oxide as electrically conductive electrode materials with excellent performance.

Acknowledgements

The authors would like to thank Sandra Schmidt and Martin Trautmann for recording the SEM and AFM images. The authors are grateful to the Deutsche Forschungsgemeinschaft (DFG) in the framework of the Cluster of Excellence Resolv (EXC1069) and the Bundesministerium für Bildung und Forschung (BMBF) in the frameworks of the project "Mangan" (FKZ 03EK3548).

References

[1] M. Smiljanic, Z. Rakocevic, A. Maksic, S. Strbac, Electrochim. Acta 117 (2014) 336-343.

[2] P. Quaino, E. Santos, Langmuir 31 (2015) 858–867.

[3] T. L. Tan, L.-L. Wang, D. D. Johnson, K. Bai, Nano Lett. 12 (2012) 4875–4880.

[4] J. Herranz, J. Durst, E. Fabbri, A. Patru, X. Cheng, A. A. Permyakova, T. J. Schmidt, Nano Energy (2016) http://dx.doi.org/10.1016/j.nanoen.2016.01.027.

[5] Refer to D. Strmcnik, P. P. Lopes, G. Genorio, V. R. Stamenkovic, N. M. Markovic, Nano Energy (2016) same issue.

[6] S. Sreekantan, E. P. San, L. C. Wei, W. Kregvirat, Adv. Mater. Res. 364 (2011) 494-499

[7] T. L. Tan, L.-L. Wang, D. D. Johnson, K. Bai, Nano Lett. 12 (2012) 4875–4880.

[8] W.-F. Chen, K. Sasaki, C. Ma, A. I. Frenkel, N. Marinkovic, J. T. Muckerman, Y. Zhu, R. R. Adzic, Angew. Chem. Int. Ed. 51 (2012) 6131–6135.

[9] J. Kibsgaard, T. F. Jaramillo, Angew. Chem. Int. Ed., 53 (2014) 14433–14437.

[10] J. Tian, Q. Liu, N. Cheng, A. M. Asiri, X. Sun, Angew. Chem. Int. Ed. 53 (2014) 9577– 9581.

[11] L. Feng, H. Vrubel, M. Bensimon, X. Hu, Phys. Chem. Chem. Phys. 16 (2014) 5917–

5921.

[12] E. J. Popczun, J. R. McKone, C. G. Read, A. J. Biacchi, A. M. Wiltrout, N. S. Lewis, R. E. Schaak, J. Am. Chem. Soc. 135 (2013) 9267–9270.

[13] Z. Xing, Q. Liu, A. M. Asiri, X. Sun, ACS Catal. 5 (2015) 145–149.

[14] D. Merki, X. Hu, Energy Environ. Sci. 4 (2011) 3878–3888

[15] D. Kong, J. J. Cha, H. Wang, H. R. Lee, Y. Cui, Energy Environ. Sci. 6 (2013) 3553–3558.

[16] Y. Yu, S.-Y. Huang, Y. Li, S. N. Steinmann, W. Yang, L. Cao, Nano Lett. 14 (2014) 553–558.

[17] A. Lukowski, A. S. Daniel, F. Meng, A. Forticaux, L. Li, S. Jin, J. Am. Chem. Soc. 135 (2013) 10274–10277.

[18] Z. Lei, S. Xu, P. Wu, Phys. Chem. Chem. Phys. 18 (2016) 70–74.

[19] G.-Q. Han, Y.-R. Liu, W.-H. Hu, B. Dong, X. Li, Y.-M. Chai, Y.-Q. Liu, C.-G. Liu, Mater. Chem. Phys. 167 (2015) 271–277.

[20] X. Yu, M. S. Prévot, N. Guijarro, K. Sivula, Nat. Commun. 6 (2015) 7596–7604.

[21] M. S. Faber, M. A. Lukowski, Q. Ding, N. S. Kaiser, S. Jin, J. Phys. Chem. C 118 (2014) 21347–21356.

[22] Q. Gong, L. Cheng, C. Liu, M. Zhang, Q. Feng, H. Ye, M. Zeng, L. Xie, Z. Liu, Y. Li, ACS Catal. 5 (2015) 2213–2219.

[23] V. Kiran, D. Mukherjee, R. N. Jenjeti, S. Sampath, Nanoscale 6 (2014) 12856–12863.

[24] C. Xu, S. Peng, C. Tan, H. Ang, H. Tan, H. Zhang, Q. Yan, J. Mater. Chem. A 2 (2014) 5597–5601.

[25] L. Yang, Q. Fu, W. Wang, J. Huang, J. Huang, J. Zhang, B. Xiang, Nanoscale 7 (2015) 10490–10497.

[26] J. Kibsgaard, Z. Chen, B. N. Reinecke, T. F. Jaramillo, Nat. Mater. 11 (2012) 963–969.

[27] J. Xie, H. Zhang, S. Li, R. Wang, X. Sun, M. Zhou, J. Zhou, X. W. D. Lou, Y. Xie, Adv. Mater. 25 (2013) 5807–5813.

[28] D. Chen, W. Chen, L. Ma, G. Ji, K. Chang, J. Y. Lee, Mater. Today 17 (2014), 184–193.

[29] Q. Liu, J. Tian, W. Cui, P. Jiang, N. Cheng, A. M. Asiri, X. Sun, Angew. Chem. Int. Ed. 53 (2014) 6710–6714.

[30] Y. Li, H. Wang, L. Xie, Y. Liang, G. Hong, H. Dai, J. Am. Chem. Soc 133 (2011)7296–7299.

[31] Z. Liu, N. Li, H. Zhao, Y. Du, J. Mater. Chem. A 3 (2015) 19706–19710.

[32] Y. Wang, J. Tang, B. Kong, D. Jia, Y. Wang, T. An, L. Zhang, G. Zheng, RSC Adv. 5 (2015) 6886–6891.

[33] K. Ullah, Z. Lei, S. Ye, A. Ali, W.-C. Oh, RSC Adv. 5 (2015) 18841–18849.

[34] Q. Feng, Y. Zhu, J. Hong, M. Zhang, W. Duan, N. Mao, J. Wu, H. Xu, F. Dong, F. Lin et al., Adv. Mater. 26 (2014) 2648-2653.

[35] J. Mann, Q. Ma, P. M. Odenthal, M. Isarraraz, D. Le, E. Preciado, D. Barroso, K. Yamaguchi, G. von Son Palacio, A. Nguyen et al., Adv. Mater. 26 (2014) 1399–1404.

[36] Z. Xing, Q. Liu, A. M. Asiri, X. Sun, Adv. Mater. 26 (2014) 5702–5707.

[37] D. R. Dreyer, S. Park, C. W. Bielawski, R. S. Ruoff, Chem. Soc. Rev. 39 (2010) 228–240.

[38] K. Andre Mkhoyan, A. W. Contryman, J. Silcox, D. A. Stewart, G. Eda, C. Mattevi, S. Miller, M. Chhowalla, Nano Lett. 9 (2009) 1058–1063.

[39] A. Dimiev, D. V. Kosynkin, L. B. Alemany, P. Chaguine, J. M. Tour, J. Am. Chem. Soc. 134 (2012) 2815–2822.

[40] B. Konkena, S. Vasudevan, J. Phys. Chem. Lett. 3 (2012) 867–872.

[41] C. Sourisseau, J. P. Forgerit, Y. Mathey, J. Solid State Chem. 49 (1983) 134−149.

[42] W. S. Hummers, R. E. Offeman, J. Am. Chem. Soc. 80 (1958) 1339.

[43] M. Hirata, T. Gotou, S. Horiuchi, M. Fujiwara, M. Ohba, Carbon 42 (2004) 2929-2937.

[44] J. O. M. Bockris, I. A. Ammar, Huq, A. K. M. S., J. Phys. Chem. 61 (1957) 879–886.

[45] J. G. N. Thomas, Trans. Faraday Soc. 157 (1961) 1603–1611.

[46] B. Wang, J. Park, D. Su, C. Wang, H. Ahn, G. Wang, J. Mater. Chem. 22 (2012) 15750–15756.

[47] Y. Ma, Y. Dai, M. Guo, C. Niu, B. Huang, Nanoscale 3 (2011) 3883–3887.

[48] C. Gong, G. Lee, B. Shan, E. M. Vogel, R. M. Wallace, K. Cho, J. Appl. Phys. 108 (2010) 123711.

[49] Y. Gorlin, T. F. Jaramillo, J. Am. Chem. Soc. 132 (2010) 13612–13614.

FIGURE CAPTIONS

Figure 1. (a) Zeta potential distribution of as exfoliated aqueous dispersions of GO and MoSSe. (b) XRD pattern of exfoliated MoSSe nanosheets and MoSSe@*r*GO composites. (c)

Raman spectra of exfoliated MoSSe nanosheets and MoSSe@*r*GO composites (d) Mo 3d core level XPS spectra of MoSSe nanosheets and MoSSe@*r*GO composites.

Figure 2. (a) SEM image of exfoliated MoSSe nanosheets. (b) TEM image of exfoliated MoSSe nanosheets. (c) SEM image of MoSSe@*r*GO composites. (d) TEM image of MoSSe@*r*GO composites.

Figure 3. (a) High magnification TEM image of a MoSSe monolayer. (b) Image of the area selected in Figure 3a. (c) HRTEM image of exfoliated MoSSe nanosheet and corresponding SAED pattern shown as inset. (d) High magnification TEM image of the MoSSe@ *r*GO composite. (e) TEM image of the area selected in Figure 3d. (f) HRTEM image of MoSSe@ *r*GO composites and corresponding SAED pattern shown as inset.

Figure 4. (a) Linear sweep voltammograms recorded at 5 mV s^{-1} for exfoliated MoS_2, $MoSe_2$ and MoSSe nanosheets. (b) Linear sweep voltammograms recorded at 5 mV s^{-1} for Pt nano powder, *r*-GO, exfoliated MoSSe nanosheets and MoSSe@ *r*GO composites. (c) Tafel plots derived from data at a slow scan rate of 1 mVs^{-1}. (d) Electrochemical durability curves recorded at 5 mV s^{-1} for MoSSe@ *r*GO composites. The inset shows the galvanostatic polarization plot recorded at a current density of 10 mA cm^{-2}.

FIGURES

Figure 1

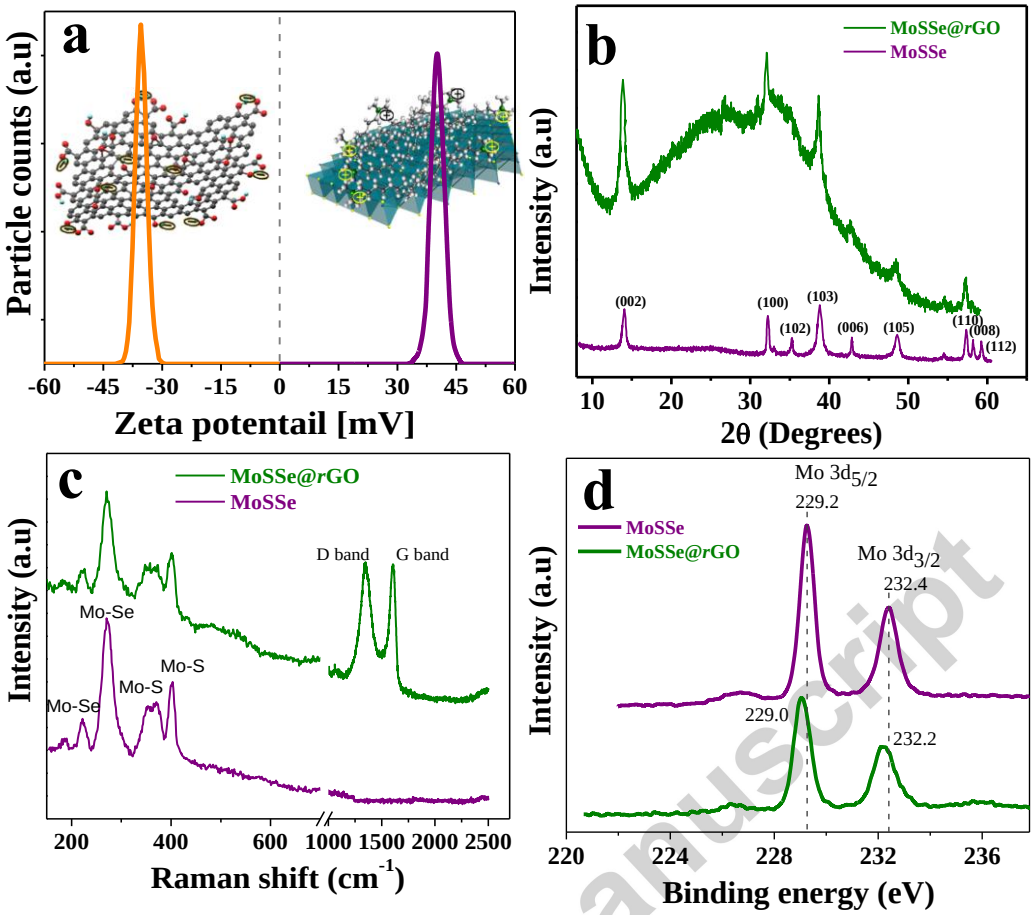

Figure 2

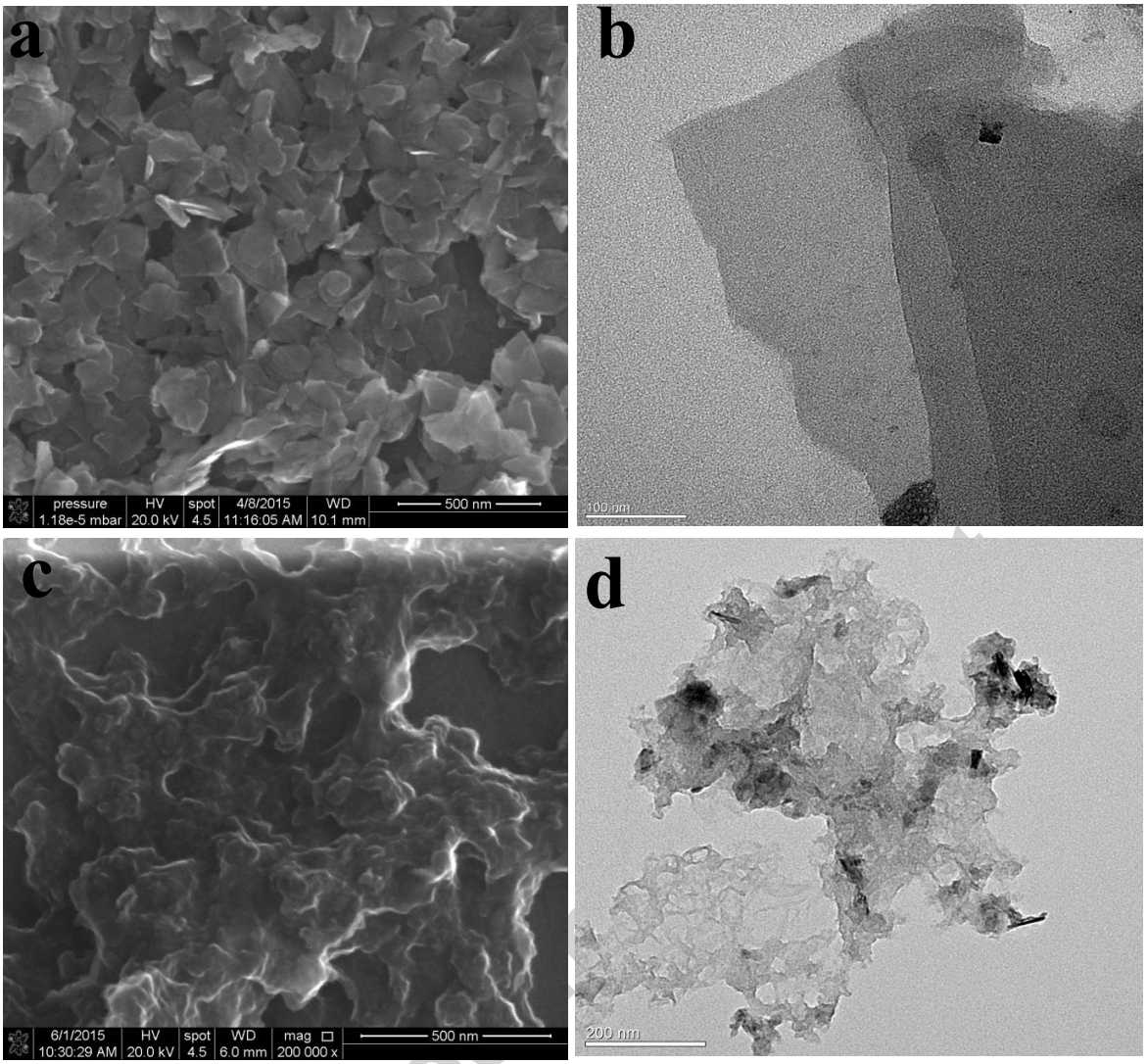

Figure 3

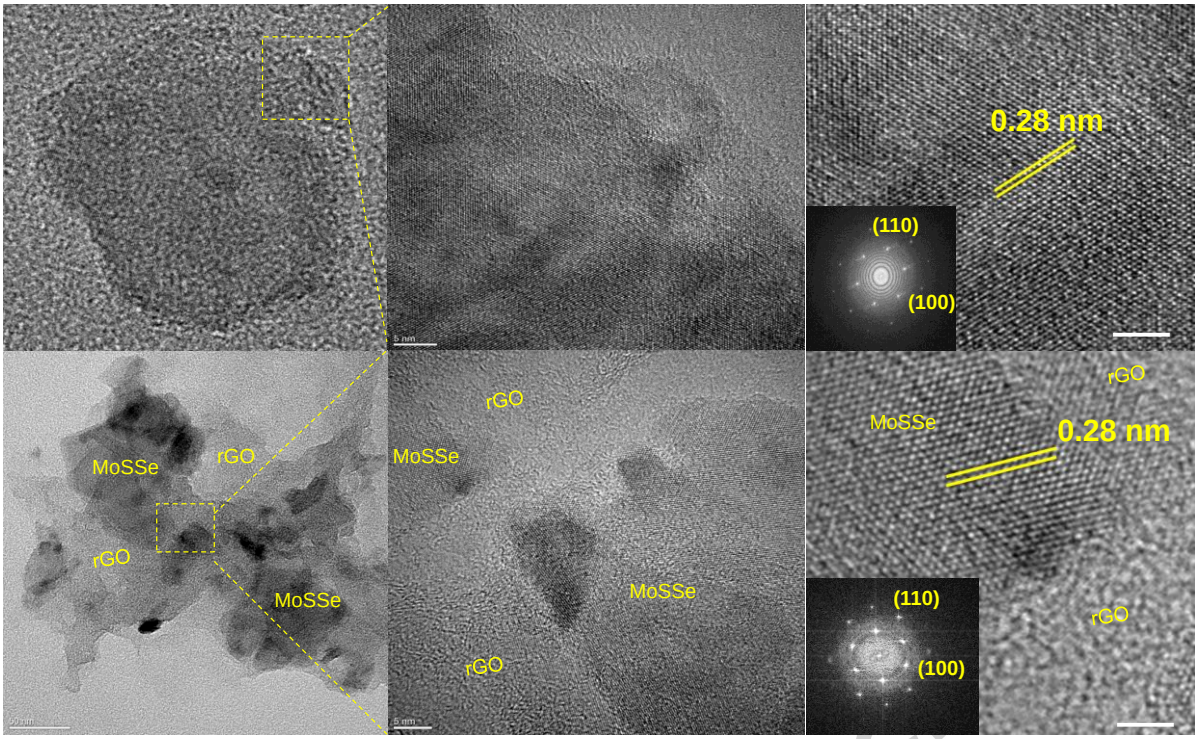

Figure 4

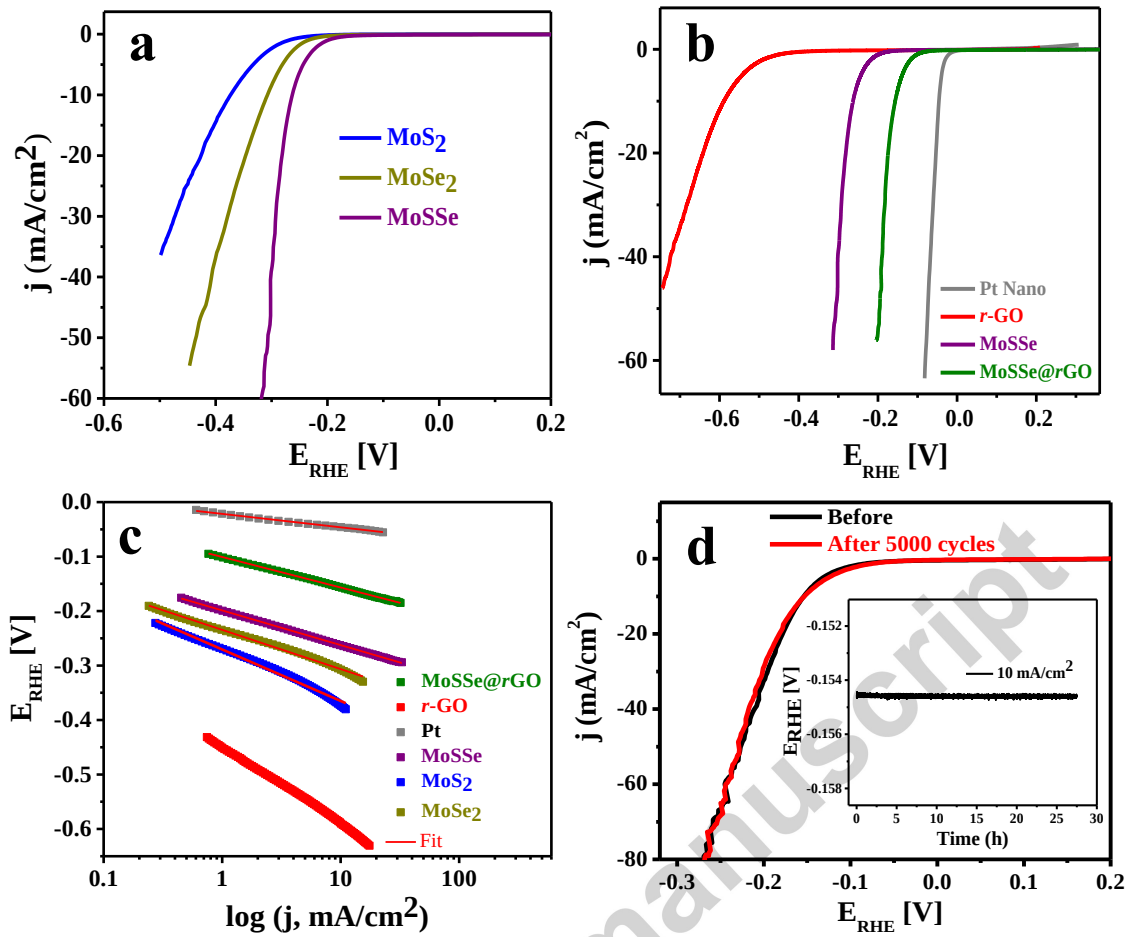

MoSSe@reduced Graphene Oxide Nanocomposite Heterostructures as Efficient and Stable Electrocatalysts for the Hydrogen Evolution Reaction

Bharathi Konkena[a], Justus Masa[a], Wei Xia[b], Martin Muhler[b], Wolfgang Schuhmann[a] *

Graphical Abstract

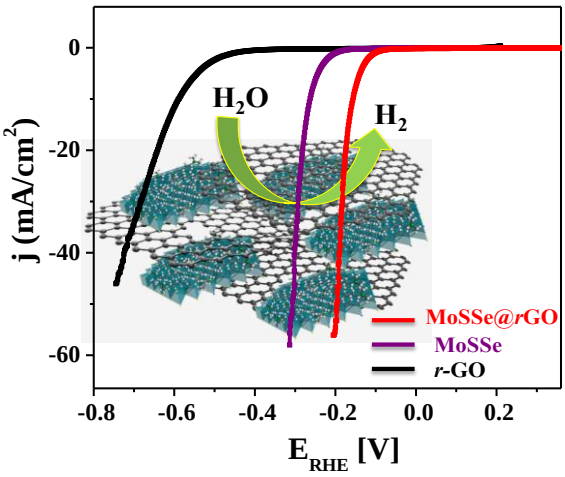

By taking advantage of the electrostatic attraction between the two oppositely charged nanosheets, MoSSe@*r*GO composite materials are obtained exhibiting superior electrocatalytic activity and stability for the HER allowing a current density of 5 mAcm^{-2} at a low overpotential of only 135 mV.

Bharathi Konkena received her Ph.D. degree in Inorganic and Physical Chemistry from Indian Institute of Science in 2014 under the supervision of Prof. S. Vasudevan. From 2015, she is working in Prof. Wolfgang Schuhmann group as a postdoctoral fellow at Electrocatalysis and Energy Conversion, the Center for Electrochemical Sciences (CES), Department of Analytical Chemistry at Ruhr-University, Bochum. Her current research interest focuses on the design, synthesis, functionalization and application of the noble-metal free nano-materials and their carbon-based composites for electrocatalysis.

Justus Masa earned a doctorate in Natural Sciences (Dr. rer. nat) from Ruhr-University Bochum, Germany, in 2012. He received a B.Sc. degree with specialization in Industrial Chemistry in 2003 and a M.Sc. degree in Chemistry in 2008 both from Makerere University, Kampala, Uganda. He is currently a Group Leader for Electrocatalysis and Energy Conversion at the Center for Electrochemical Sciences (CES), Department of Analytical Chemistry at Ruhr-University Bochum and was a Visiting Scholar in the Physical and Theoretical Chemistry Laboratory at the University of Oxford in the summer of 2013 in the group of Prof. Richard Compton. His research interests include electrocatalysis, especially the rational design of low-cost catalysts for fuel cells, electrolyzers and nanomaterials design for electrochemical energy systems.

Wei Xia studied chemistry at Tongji University in Shanghai from 1993 to 1998. After working for four years in Shanghai, he moved to Germany in 2002 and obtained his Master in polymer science from Martin-Luther University Halle--Wittenberg in 2004. He then moved to Ruhr-University Bochum and obtained his PhD in heterogeneous catalysis in 2006

under the supervision of Prof. M. Muhler. Since 2008 he has been a group leader in the Laboratory of Industrial Chemistry, Ruhr-University Bochum.

Martin Muhler studied chemistry at the Ludwig Maximilians University in Munich and received his PhD in 1989 at the Fritz Haber Institute of the Max Planck Society in Berlin with Prof. Dr. G. Ertl. After two years postdoctoral research at the Department of Fundamental Research in Heterogeneous Catalysis at Haldor Topsøe A/S in Denmark, in 1991 he became group head at the FHI Berlin. In 1996, he completed his habilitation in Industrial Chemistry at the TU Berlin, and was appointed full Professor of Industrial Chemistry at the Ruhr University Bochum. In 2013, he was elected Chairman of the German Catalysis Society.

Wolfgang Schuhmann studied chemistry at the University of Karlsruhe, and completed his PhD with F. Korte in 1986 at the Technical University of Munich. After finishing his habilitation at Technical University of Munich in 1993, he was appointed professor for Analytical Chemistry at the Ruhr-University Bochum in 1996. He is a fellow of the Royal Society of Chemistry (2005) and the International Society of Electrochemistry (2012). He has received the Biosensors & Bioelectronics Award (2000), the Julius von Haast Fellowship Award (2008), the Katsumi Niki Prize of Bioelectrochemistry (2012), the Howard Fellowship of the University of New South Wales, Sydney (2014) and the Heyrovsky-Ilkovic-Nernst-Lecture of the GDCh, the Czech and the Slovak Chemical Societies (2014).

Research highlights

- Novel approach for synthesis of thin composite sheets of molybdenum sulphide supported on graphene oxide
- Thin composite films are formed by exploiting electrostatic interaction of oppositely charged groups
- The composite exhibits outstanding activity and stability in catalyzing hydrogen evolution under acidic conditions